# Novel metal-carbon nanomaterials: A review on covetics

**Mete Bakir, Iwona Jasiuk***

*Department of Mechanical Science and Engineering, University of Illinois at Urbana-Champaign, 1206 W. Green Street, Urbana, 61801, IL, USA*

*Corresponding author: Tel: (+1)-217-333-92-59; E-mail: ijasiuk@illinois.edu

**Received: 30 December 2016, Revised: 18 February 2017 and Accepted: 09 April 2017**

DOI: 10.5185/amlett.2017.1598
www.vbripress.com/aml

## Abstract

Covetics are a novel class of metal-carbon nanomaterials. The covetics are fabricated using a conventional induction furnace wherein an electric current is applied into an activated carbon infused molten metal medium. In situ generated arc discharge induces a chemical conversion reaction where the amorphous carbon attains a crystalline structure and forms covalent bonding with host metal matrix. Such fabrication approach also promotes higher carbon solubility in the molten metal than that in traditional metal-carbon alloys. Nanoscale structure analyses revealed single-phase carbon-metal lattice morphologies in the covetics. The covetics have also been shown to possess improved thermos-physical properties as compared to their parent metals. We herein present a review of the literature on the covetics. First, we introduce the covetic materials, and then provide a brief overview on metal-carbon nanocomposites. Then, we summarize experimental results on covetics. Finally, we discuss characterization challenges and future directions in the covetics research. Copyright © 2017 VBRI Press.

**Keywords:** Covetics, metal-carbon nanomaterial, nanoscale structure, mechanical properties.

## Introduction

A decade ago Jason Shugart and Roger Scherer from Third Millennium Materials ($TM^2$), LLC developed a new method to manufacture high carbon content metal compositions [**1, 2**]. These materials possess single-phase morphology comprising of nanocarbon reinforcement in metal lattice structure such that the carbon does not separate from the metal upon remelting and subsequent resolidification processes. This behavior has been attributed to the formation of an *in-situ* covalent bonding between the carbon and the metal. During the fabrication process, electric arc induces chemical conversion of the amorphous activated carbon into crystalline carbon form such that the carbon thereby interacts with the metal lattice and forms a new hybrid nanoscale morphology. This novel carbon-metal material was named "covetic" referring to a hypothesized covalent bonding of the carbon atoms to the metallic crystalline structures. The covetics manufacturing method involves the use of a conventional induction furnace, wherein the metal is melted inside a graphite crucible. Then, activated carbon particles are blended into the molten metal while it is being stirred and a sufficient electric current is applied via carbon electrodes to realize such chemical conversion reaction. So far, covetics were mainly demonstrated with the use of micron-sized amorphous activated carbon particles infused into about twenty metals including aluminum, copper, silver, zinc and tin [**3**].

Carbon incorporation into a metal matrix may yield improved properties as compared to base metals. For example, aluminum carbide, obtained through a chemical reaction between aluminum and carbon, possesses superior hardness and higher melting point to the soft and low-temperature malleable parent aluminum. Also, steel, obtained through dissolving carbon in iron, attains better structural properties and oxidative corrosion resistance than iron. However, most metals pose chemical inertness to carbon which yields low, if not negligible, carbon solubility. Namely, copper has around 6-8 ppm [**4**], while nickel has about 1 wt.% carbon solubility [**5**]. Iron has higher solubility with steel having up to 2.14 wt.% and cast iron up to 6.7 wt% [**6**]. The covetics have been shown so far to have up to 15 wt.% carbon solubility which realizes a significant advancement for the metal-carbon materials.

Alternatively, to overcome the carbon solubility issue, metal-carbon composites have been fabricated by incorporating solid-phase carbon nanoparticles via various processing techniques which include chemical vapor deposition (CVD) [**7**], spark plasma sintering [**8**], melt processing [**9**] and thermal spraying [**10**], among others. Utilizing such methods, higher carbon contents can be realized in metal-matrix composites which in return may yield notable improvements in physical properties. For example, graphene was grown via CVD on copper powder and such powder generated a composite material with 39% improvement in hardness, in comparison to a base copper [**11**]. Also, carbon nanotube filled aluminum, prepared

using mechanical ball milling and hot pressing techniques, yielded five times higher hardness and seven times higher flexural strength [**12**]. In another work, 3 vol.% of carbon nanotube infused aluminum matrix showed higher yield strength and hardness than base material [**13, 14**]. Copper with incorporated carbon nanotubes had almost equivalent conductivity to pure copper [**15**]. Graphene infused copper system displayed dislocation inhibited strengthening effects [**16**]. Also, metal oxide graphene compositions showed enhanced electrochemical capacitance which denoted their potential for energy storage applications [**17**].

Thus, enhancements in material properties could be achieved by utilizing the above techniques to attain higher carbon content in metal matrix composites. Yet, poor interfacial bonding between the carbon fillers and the host metal matrix limits benefits which could be obtained from the added carbon. Thus, the covetic materials enabling *in-situ* generated interfacial bonding and unique single-phase lattice structure should positively alter thermo-physical properties. We hereon summarize experimental findings on the covetics, in chronological order, to highlight their promising characteristics.

## Experimental Findings

The very first work on the covetics was published by Brown *et al.* in 2011 [**18**]. In that study, physical properties of a 3 wt.% carbon incorporated aluminum alloy (Al6061) covetic material were investigated and compared with a bare aluminum alloy parent material. Density was measured using a gas pycnometer where only an infinitesimal difference was observed between the covetic and parent materials. Predicted by a rule of mixtures, the actual volume fraction of the carbon content was 1.17 vol.% for the reported as-manufactured ratio of 3.56 vol.% in the covetic material. Thus, the covetic materials can be described by either target carbon denoting carbon amount used during fabrication, or an actual carbon percentage measured via spectroscopic techniques. Yet, precise quantification of the carbon content in covetics still remains to be a challenge. Vickers microhardness measurements yielded 23.4% higher average hardness values for the covetic material, which was attributed to the presence of the carbon nanoparticles. It is worthwhile to mention that hardness was observed to increase towards outer regions of the circular cross-section cut samples, indicating a nonuniform distribution of carbon. Following hardness measurements, images taken on indented regions displayed intact carbon aggregations, which were speculated to happen due to an incomplete chemical conversion reaction. More importantly, electron beam backscatter diffraction (EBSD) analysis showed notable grain-size differences between the covetic and parent materials wherein the former had fine-grained (1-30 μm diameter) regions with strong orientation dependence, whereas the latter had 100-200 μm diameter large grains with random orientations. Furthermore, four-probe method electrical conductivity measurements (according to ASTM B193) demonstrated that as-extruded covetic aluminum reached 67.3±3% IACS (International Annealed Copper Standard). Upon a T6 heat treatment, the electrical conductivity reduced to 47.81±3% IACS and essentially became comparable to a bare aluminum alloy with same heat-treatment. Quasi-static tensile tests showed that the yield and ultimate strengths of the covetic material were about 30% higher than those of the base aluminum alloy as shown in **Fig. 1**. However, upon a T6 heat treatment, although material properties substantially increased, no noticeable differences were observed between the covetic and non-covetic materials. Split Hopkinson pressure bar (SHPB) measurements, which give strain rate dependency of mechanical properties, showed no significant differences between the T6 conditioned covetic and parent materials. Lastly, differential thermal analysis (TGA) gave higher solidus temperature (619°C) for the covetic material than the literature value of the parent T6-conditioned material (582°C). These preliminary measurements demonstrated promising results for covetics, but underlying reasons were not comprehensively discussed.

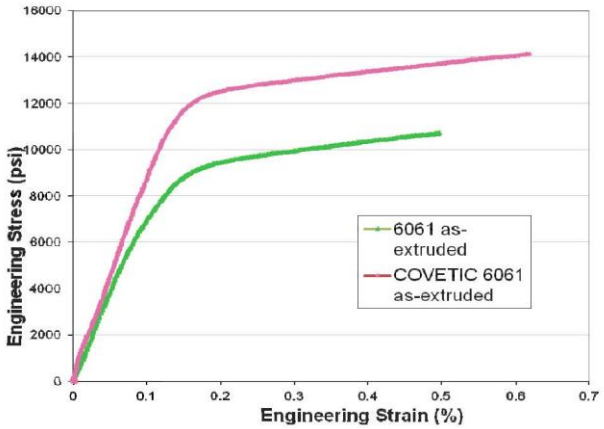


**Fig. 1.** Tensile characteristics of parent and covetic materials where the covetic material obtained higher yield and ultimate strength [**18**].

Following that study, Nilufar *et al.* [**19**] and Jasiuk *et al.* [**20**] presented experimental results on warm-rolled (T0 conditioned) Al7075 covetic materials having 0, 3 and 5 wt.% target carbon compositions. They measured 0.8, 2.2 and 4 wt.% actual carbon contents for 0, 3 and 5 wt.% target compositions, respectively, using electron dispersive spectroscopy (EDS). Structural density measurements using the buoyancy technique did not show any significant differences among all three compositions, which was attributed to lower actual carbon quantities. Yet, Vickers and Rockwell hardness tests of the covetics yielded improved properties where the hardness increased by 30% in 5 wt.% target carbon content covetic samples as shown in **Fig. 2**. Similarly, nanoindentation measurements displayed a 43% increase in hardness but no improvement in a reduced elastic modulus. Also, tensile test showed that covetic materials with 5 wt.% target carbon content could attain an ultimate strength as high as bare T6-tempered Al 7075. In other words, about 40% strength increase was observed in the corresponding covetic material. Additionally, scanning electron microscopy (SEM) images revealed brittle fracture formed with an increased carbon content. Mechanical property results were comparable to

 

those reported in [**18**], showing notable improvements for the covetic materials.

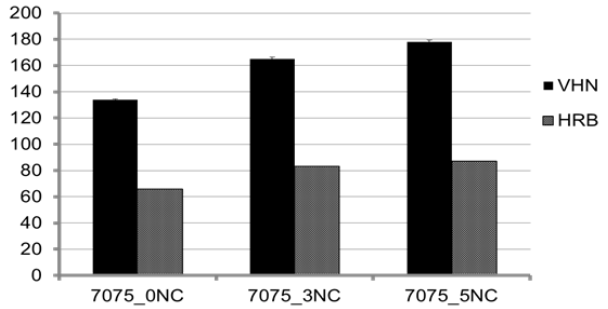


**Fig. 2.** Vickers (VHN) and Rockwell (HRB) hardness measurements on Al7075 covetics [**19**].

Salamanca-Riba *et al.* [**21**] studied the form of carbon in the covetics using several different experimental techniques. In that study, they investigated 2 wt. % and 5 wt.% copper (Cu) covetics, 3 wt. % silver (Ag) covetics and 3 wt.% aluminum alloy (Al6061) covetics, as expressed by their target contents. Using SEM, two different carbon domain types were detected on 3 wt.% Al6061: 50-200 nm size "particle nanocarbon", and 5-100 nm size "lattice structure nanocarbon". Wherein, the former was amorphous and well distributed into the matrix, and the latter formed an inter-connected network. In that regard, high-resolution transmission electron microscopy (HRTEM) images of 5 wt.% Cu110 covetic sample displayed nanocarbon regions observed as weak satellite spots in diffraction patterns, where high carbon content was separately detected via EDS. As well, lattice structure nanocarbon yielded stripe forms in the aluminum covetic, as detected through a high angle annular dark field (HAADF) technique. Similarly, HRTEM of silver covetic demonstrated alternating graphene layers as formed in between (111) silver planes. Electron energy loss spectroscopy (EELS) data showed peak formations around 284eV denoting $sp^2$ bonded carbon which indicates graphitic structures forming in all three covetic configurations. Supporting the EELS results, Raman spectra on Al6061 covetics revealed characteristic D-band and G-band where the G-band defines graphene morphology. Also, an x-ray photoelectron spectroscopy (XPS) depth profiling of the Ag covetic showed a constant carbon content (0.71 wt. %) following a sputtering process. It is imperative to highlight that covetic surfaces were observed to contain hydrocarbon contaminations that after sputtering processes significantly reduced the initially detected carbon content. Finally, mechanical tests showed improved properties of Al covetics, validating earlier findings. This study demonstrated use of various spectroscopic techniques to analyze form of the carbon in the covetic structures, which paved way for further characterization of the carbon in the covetics.

Then, Forrest *et al.* [**22**] investigated properties of Cu and Al covetics with various carbon contents. They reported that LECO and glow discharge mass spectroscopy (GDMS) methods were only able to detect trace amounts of carbon, which corresponded to the unconverted carbon. XPS and EDS gave carbon quantities of 3.5 and 3.78 wt.%, respectively, for a 5 wt.% target amount in Cu covetics. Also, solidus temperatures of both Cu and Al increased as compared to literature values. Density of a 3.5 wt.% copper covetic, measured using a gas pycnometer, was lower than one of pure copper. Thermal conductivity of Cu covetic with actual 0.057 wt.% C was tested using two different techniques: steady state measurement (ASTM E1225) and laser flash diffusivity technique (ASTM E1461). The latter method demonstrated 50% higher thermal conductivity values than of the parent Cu material, while the former showed anisotropy in this thermal property. Electrical conductivity of 3 wt.% Al covetic was measured using the four-probe technique wherein as-extruded covetic yielded the highest electrical conductivity, 67.3% IACS, higher than of a conventional Al 6061 alloy. Regarding mechanical properties, as-extruded 3 wt.% Al covetic possessed 30% higher yield strength than its parent material. However, upon T6 heat treatment, both electrical and mechanical properties were very similar to the properties of their base material. It was concluded that resistance of as-extruded material to grain-coarsening resulted in the higher mechanical strength where heat treatment relaxed and minimized that effect.

Brown *et al.* compiled findings on physical, mechanical and electrical properties of 3 wt. % Al 6061 covetics [**23**]. They evaluated both parent and covetic materials being as-extruded (T0) and heat-treated to T6 condition. LECO analysis showed that an unconverted carbon content in this 3 wt% C covetic material was 0.3 wt. %. SEM images displayed nanocarbon particles ranging between 5-200 nm in diameter, where complementary EDS mapping revealed both converted and unconverted carbon sites. Similar to the prior results, this work reported no significant density change in the covetics. Yet, in terms of hardness, as reported in [**18**], about 23 % hardness increase occurred in the T0 covetics which was correlated with the reduced grain size. Regarding tensile properties, T0 covetic material demonstrated 29% higher ultimate strength than the parent material and yield strength was 30% greater. Electrical conductivity measurements showed 20% higher conductivity of a T0 covetic than of its parent material. However, upon the T6 heat treatment such differences were removed. Yet, quality of surface finishing increased the conductivity by about 8% in the T6 condition. Also, strain rate dependency measurements were conducted, similar to those in [**18**], where the T0 covetic showed a 40% higher strength at increased strain rates while the T6 covetic did not reveal any dependence on strain rates, correlating with prior findings.

On top of these pioneering works, researchers at the University of Science and Technology (AGH) in Krakow first time independently synthesized copper covetics [**24**]. They utilized activated carbon (0.83 and 2 wt. %.) and carbon nanotube (0.77 wt. %) reinforcements. Fabrication protocols and processing parameters are detailed in the study. Chemical analyses demonstrated very low oxygen content, and, more importantly, carbon contents of the samples were comparable with corresponding amounts added during the fabrication. Activated carbon

 

incorporated covetics had lower density than the pure copper while CNT added covetics had similar density to the one of the pure copper. Hardness values of the covetics were lower than those of the pure copper, which was not consistent with previous findings. Electrical conductivities of the three material types were close to those of pure copper, which was impressive as presence of impurities was reported. Using secondary-ion mass spectroscopy (SIMS), very small amount of carbon was detected in the CNT covetic, while carbon black covetic samples had a more viable carbon content. Microstructural analysis showed secondary darker domains which were attributed to the presence of a graphitic carbon.

In a follow-up work, the AGH researchers adopted a similar manufacturing method and they performed structural characterizations on as-cast covetic samples and extruded wires from covetic samples [**25**]. During the fabrication process, argon gas protection was provided to prevent oxidation and combustion of the carbon at high temperatures. Covetic samples having 2-3 wt.% activated carbon were fabricated. The study provided detailed information regarding processing parameters. LECO-optical emission spectroscopy (OES) coupled analyses showed oxygen content at trace levels, with no carbon content detected. SIMS visually demonstrated presence and distribution of the carbon in the samples wherein lower carbon content and uneven distributions were also observed for different processing parameters. Densities of the samples were measured to be lower than of the pure copper. Hardness of the higher carbon content sample was 20% lower than the lower carbon content samples, contradicting previous findings. Electrical conductivity was measured as high as 100.17% IACS in spite of impurities. Regarding the processed wires, tensile strength and yield strength were observed to decrease upon annealing which validated the above findings that thermal treatment reduces mechanical properties. Yet, electrical properties were preserved upon annealing.

Salamanca-Riba *et al*. characterized Ag-covetics with 3 wt. and 6 wt.% activated carbon [**26**]. X-ray photoelectron spectroscopy (XPS) depth profiling was utilized to analyze distribution of the carbon in the silver matrix (3 wt.%). They observed that after 1 minute of Ar ion sputtering the carbon content remained almost constant at 1 wt.%, indicating effective removal of surface hydrocarbon contaminations. X-ray diffraction (XRD) studies on a 6 wt.% covetic sample showed that the silver lattice structure did not change with a carbon infusion. It is important to note that no peaks of carbon or graphene (crystalline structure) were observed. Additionally, in TEM, they observed weak spots (patterns) between <220> Ag which indicated a carbon structure, as also validated by EELS. Through some calculations, interplanar distance of the weak spots was found to be closely comparable to $<10\bar{1}0>$ interplanar distance of the graphite, yet with 13% strain applied on the carbon structure. Considering lattice and thermal expansion coefficient mismatches between carbon and silver, it was concluded that such a high strain formed due to an epitaxial rearrangement of a lattice structure in the covetics. Based on that it was concluded that the carbon structure formed alternating layers of graphene between atomic planes of silver as shown in **Fig. 3.** Raman spectroscopy of 6 wt.% Ag covetic showed presence of carbon via illustrative D and G (disornanocrystalline graphite) characteristic peaks of a $sp^2$ bonding. The position of 1600 $cm^{-1}$ as compared to 1540 $cm^{-1}$ of pristine graphene, was attributed to highly disordered carbon forms in the metal as well as an induced strain. The D-band at 1334 $cm^{-1}$, on the other hand, corresponded to formation of a defective carbon structure. The carbon structure was also evidenced by XPS spectra exhibiting a carbon peak at 284.4 eV. Additionally, EELS showed a slight peak at 284 eV corresponding to graphitic carbon. Adding carbon into the silver increased melting temperature of the covetics by 15°C (from 961.78°C to 976.5°C). Additionally, upon consecutive heating cycles, no further change in the melting temperature and materials weight were observed meaning that the carbon did not phase separate during heating/melting processes due to a strong bond with Ag matrix. Electrical conductivity of 6 wt.% covetic samples was measured to be 5.62 x $10^7$ S/m as compared to 6.2 x$10^7$ S/m of the pure silver.

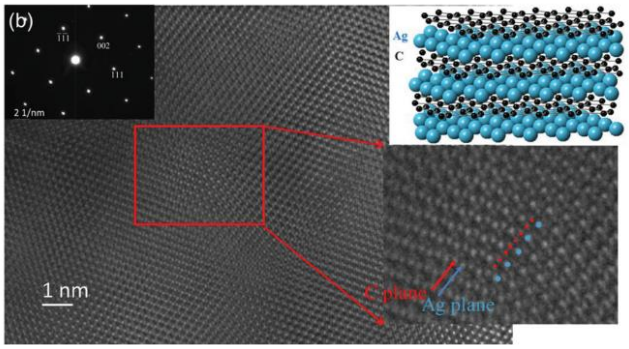


**Fig. 3.** HRTEM image and diffraction pattern of 3 wt.% Ag covetic [**26**].

Isaacs *et al*. characterized copper covetics with 5 wt.% carbon [**27**]. An $(0\bar{1}1)$ electron diffraction pattern displayed weak satellite spots, similar to the previous study [**26**], corresponding to modulation of 1.6 nm size, as observed in HRTEM along with detected high carbon content. It was concluded that during the covetics fabrication process, high-level of the current led to self-arrangement of the carbon structures in the copper matrix. XPS depth profiles and EDS demonstrated the carbon content close to a target value. Next, thin films (18 nm) of covetics on Si substrate were obtained using an e-beam deposition technique. Transmittance measurements revealed that copper covetics (with 5 wt.% carbon) were more transparent than the parent copper. Also, it was observed that as the carbon content increased, the thin films became more transparent. This result was attributed to special interstitial placement of the carbon C in the Cu lattice that resulted in a lower reflection coefficient. With regard to electrical conductivity measurements, the covetic films showed lower and long-term stable resistivity than the pure copper film of the same thickness. The covetic films preserved their resistivity up to 80 days, while pure copper films were observed to degrade quickly. Wherein,

 

the copper covetics inherently generated a resistance to oxidation due to the presence of carbon-copper bonds.

More recently, Ma *et al.* reported three-dimensional (3D) nanoscale imaging of carbon features in the copper covetics with 0.21 wt.% C using synchrotron hard X-ray nanotomography [**28**]. SEM images further displayed micron-size spherical features, having notable oxygen content and no difference in the carbon content as shown in **Fig. 4**. Those features were attributed to form during the covetics fabrication process. In bright field TEMs, evidencing the SEM/EDS, the inclusions had higher oxygen content than the copper matrix. Scans of X-ray transmission micrographs revealed also formations of those features at various rotation angles. Additionally, X-ray radiographs clearly display those nanoscale features.

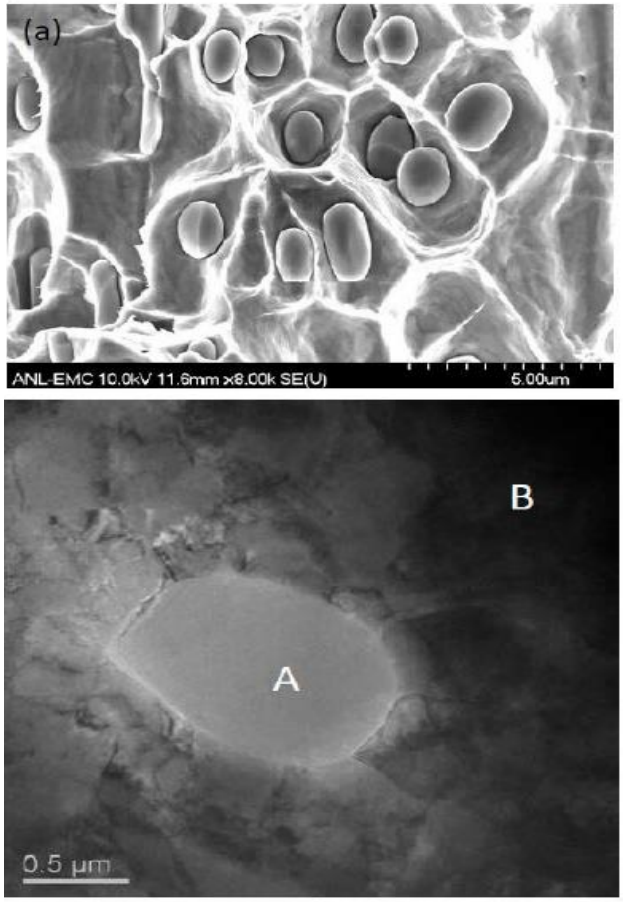


**Fig. 4.** SEM (top) and TEM (bottom) images taken on the covetics [28].

Jaim *et al.* studied the covetic structure, C-C bonding, and dispersion of carbon and bonding of carbon to aluminum matrix [29]. Using high angle HADDF mode in TEM, they demonstrated presence of folded ribbon-like structures in 3 wt.% Al 6061 covetic. The nanostructure was detected to have high concentration of carbon and oxygen using EDS. In TEM, weak spots were observed in diffraction spectra, as reported earlier, which were attributed to a preferential orientation of carbon in the aluminum lattice. Note that, some amorphous carbon was also detected in the same spectra. EELS spectrum imaging confirmed presence of the $sp^2$ bonding with a sharp edge at 284 eV evidencing conversion reaction. EELS C-K mappings also revealed presence of the nanoribbons. Additionally, Raman spectra taken on the aluminum covetics displayed strong peaks of D and G bands highlighting presence of carbon in the structure. Wherein, the intensity ratio between D and G peaks indicated formation of a graphitic disorder. They performed surface measurements on the covetics using AFM-KPFM technique that phase maps displayed darker spots with low surface potential corresponding to carbon nanoribbons being distributed in the matrix. Carbon content in the covetics was measured using XPS which again demonstrated carbon content being lower than the target carbon values. Regarding morphological analysis, XRD spectra, in particular, did not reveal any evidence of carbon or allotrope formations in the covetic structure as shown in **Fig. 5.** Yet, the covetic samples were polycrystalline having preferential orientations, as indicated by their changing indicial intensities with respect to different orientations. Also, it was observed that lattice constant as well as average crystallite size of the covetic structure decreased with an increased carbon content. Notable increases in ultimate tensile strength and hardness of the covetics were also observed.

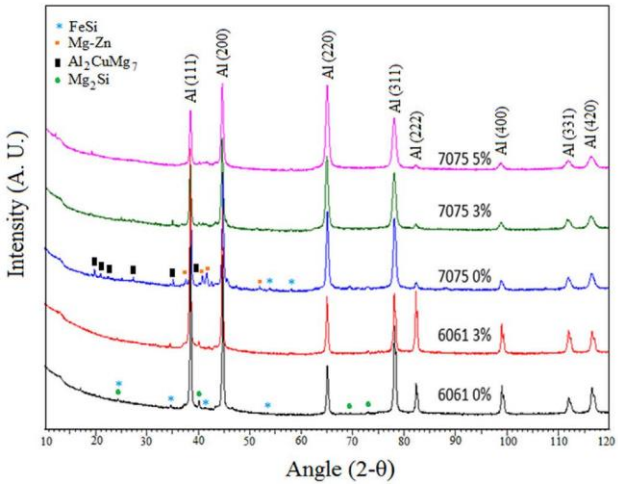


**Fig. 5.** XRD spectra of covetics [**29**].

Additionally, Balachandran *et al.* studied copper covetics with 3 wt.% carbon [**30**]. XRD results on both parent and covetic materials displayed impurities, wherein they also observed a $Cu_2O$ formation in the parent material, but not in the covetic. Densities of the parent material and the covetic material were close, yet both were above the pure copper density. In SEM, both samples had similar grain sizes (~1 µm). In DSC scans, they observed two peaks: low-temperature peak, corresponding to solidus temperature of $Cu_2O$, and higher temperature peak of copper. Regarding electrical conductivity, the parent material demonstrated 93.2% IACS while the covetic had 99.5% IACS. Parent copper and covetic materials exhibited similar thermal conductivities, where the covetic samples had 10% higher conductivities.

Jaim *et al.*, in a followup study, reported Raman studies on Al and Ag covetics analyzing $sp^2/sp^3$ bonding, strain, defects, oxidation and crystalline sizes of nanoribbons

 

[**31**]. In Raman measurements, they confirmed that 3 wt.% Al covetic possessed the characteristic G and D peaks, along with some amorphous carbon. Intensity variations observed through Raman mapping demonstrated unstrained condition for the G peak, whereas the D peak revealed strained carbon forms. Additionally, EELS imaging demonstrated formation of oxidation on the covetic samples. Through C mapping, nanoribbon like features were observed, at 284 eV, indicating $sp^2$ carbon. Also, Raman spectra taken on the pure Ag and 6wt.% Ag covetic samples displayed blue shifts in the G band which indicated compressive strains induced on the carbon. Interestingly, it was reported that strained regions were surrounded by unstrained regions wherein the highest strain was located in central carbon spots. As expected, variations in the D peak indicated presence of both $sp^2$ and $sp^3$. AFM/KPFM maps showed darker regions indicating presence of carbon along with some ribbon like structures having low surface potential. EELS of the 6 wt.% Ag covetic showed carbon rich regions along with the observed peaks at 284 and 290 eV indicating a $sp^2$ carbon structure.

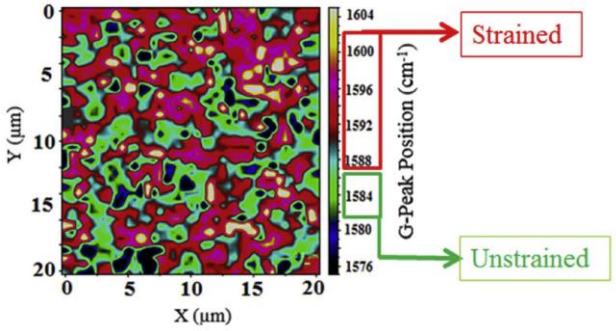


**Fig. 6.** G-peak mapping of 6 wt.% Ag covetic [**31**].

## Conclusions and future perspectives

Macroscopic quantification of the carbon content is of key importance for determination of composition-structure-property relations of the covetics. However, quantitative characterization of the carbon content still remains a challenge. As discussed, target carbon contents utilized during processing are not necessarily the measured values of fabricated materials. So far, EDS and XPS measurements provided valuable information in that regard. Yet, those techniques are limited to localized surface measurements. Hence, EDS/XPS are not sufficient to obtain the overall macroscopic (bulk) carbon content in the covetics. Also, covetics are subjected to detector-originated carbon contaminations within the EDS and XPS chambers. Thus, such measurements require simultaneous use of calibration samples to obtain accurate carbon content measurements. Combustion-based bulk techniques of LECO and GDMS did not provide valuable insights into the carbon content, which is attributed to strong bonding between carbon and metal in the covetic materials. Although density measurements appear to be a viable approach to quantify the carbon content, the predicted carbon contents via such method do not agree with the ones measured via spectroscopic techniques. Although the outcome is more likely due to porosity in the covetics, more detailed analyses of this concept could be pursued.

Furthermore, as XPS measurements demonstrated, surface hydrocarbon contamination is predominant in covetics. Although TEM and Raman measurements demonstrated crystalline carbon morphologies, XRD measurements so far did not validate such results nor displayed characteristic carbon peaks. It could be attributed to lower carbon content being below detection limits of the XRD instrument. However, XRD provides consistent results with EBSD regarding the reduced grain size in the covetics.

SIMS [**24**] and x-ray micro-computed tomography (micro-CT) [**28**] techniques provided valuable information on imaging of carbon dispersion and they could be complementarily utilized. Besides, the use of SIMS/X-Ray micro-CT could be further extended to quantification of the macroscopic carbon content.

Secondly, several studies provided valuable insight into form and bonding of carbon nanoparticles. Yet, comprehensive understanding of those outcomes and of the conversion reaction of the covetics is still lacking.

Another important issue is thermal stability of carbon particles (mostly activated carbon) in high melting temperatures of metals. Such high temperatures may cause rapid thermal decomposition of the added carbon resulting in abrupt weight reductions. Wherein, thermal stability of the carbon should be analyzed with respect to processing temperature and time along with heating chamber ambient (air or vacuum). Indeed, lower values measured for carbon content could stem from decomposition of carbon particles during manufacturing.

Most studies showed improvement in mechanical properties of covetics. However, reasons for these improvements are not yet fully understood. Also, upon heat treatment, covetics were observed to lose such improved mechanical properties. So, to establish mechanical property comparison, both covetic and parent materials should be processed under same thermal conditions. In addition, not all studies confirmed the previously reported improvements in electrical and thermal conductivities. Thus, further studies on electrical and thermal conductivities of covetics are needed.

Another pressing need is to understand effects processing parameters during the covetics manufacturing on covetics properties so these materials could reach their optimum performance.

In summary, covetics have promising physical properties surpassing those of the corresponding bare metals. With so far demonstrated characteristics, covetics possess potential to address needs in cutting-edge applications. However, further research is needed before that can be fully accepted and used in industrial applications.

**Acknowledgments**

This research was supported by the DOE-STTR grant (DE-SC0015115) and by funding from the Air Conditioning and Refrigeration Center at the University of Illinous at Urbana-Champaign.

 

**References**


1. Shugart, J. V.; Scherer, R. C.: Metal-carbon compositions. U.S. Patent 8541335 B2, **2013**.
2. Shugart, J. V.; Scherer, R. C.: Copper-carbon composition. U.S. Patent 20100327233 A1, **2010**.
3. Scherer, R. C.; Shugart, J. V.; Lafdi, K. New class of metallic nanocomposites - nanocarbon metals. *Materials Science & Technology Conference and Exhibition* **2009**.
4. López, G. A.; Mittemeijer, E. J. The solubility of C in solid Cu. *Scripta Mater* **2004**, *51*, 1. **DOI:** 10.1016/j.scriptamat.2004.03.028
5. Lander, J. J.; Kern, H. E.; Beach, A. L. Solubility and diffusion coefficient of carbon in nickel: reaction rates of nickel-carbon alloys with barium oxide. *Journal of Applied Physics* **1952**, *23*, 1305-1309. **DOI:** 10.1063/1.1702064
6. Speer, J.; Matlock, D. K.; De Cooman, B. C.; Schroth, J. G. Carbon partitioning into austenite after martensite transformation. *Acta Materialia* **2003**, *51*, 2611. **DOI:** 10.1016/S1359-6454(03)00059-4
7. He, C.; Zhao, N.; Shi, C.; Du, X.; Li, J.; Li, H.; Cui, Q. An approach to obtaining homogeneously dispersed carbon nanotubes in Al powders for preparing reinforced Al-matrix composites. *Adv Mater* **2007**, *19*, 1128-1132. **DOI:** 10.1002/adma.200601381
8. Kwon, H.; Estili, M.; Takagi, K.; Miyazaki, T.; Kawasaki, A. Combination of hot extrusion and spark plasma sintering for producing carbon nanotube reinforced aluminum matrix composites. *Carbon* **2009**, *47*, 570. **DOI:** 10.1016/j.carbon.2008.10.041
9. Hashim, J.; Looney, L.; Hashmi, M. S. J. Metal matrix composites: production by the stir casting method. *Journal of Materials Processing Technology* **1999**, *92–93*, 1-7. **DOI:** 10.1016/S0924-0136(99)00118-1
10. Laha, T.; Agarwal, A.; McKechnie, T.; Seal, S. Synthesis and characterization of plasma spray formed carbon nanotube reinforced aluminum composite. *Materials Science and Engineering: A* **2004**, *381*, 249-258. **DOI:** 10.1016/j.msea.2004.04.014
11. Koltsova, T. S.; Nasibulina, L. I.; Anoshkin, I. V.; Mishin, V. V.; Kauppinen, E. I.; Tolochko, O. V.; Nasibulin, A. G. New hybrid copper composite materials based on carbon nanostructures. *Journal of Materials Science and Engineering B* **2012**, *2*, 240.
12. Kwon, H.; Lee, G.-G.; Kim, S.-G.; Lee, B.-W.; Seo, W.-C.; Leparoux, M. Mechanical properties of nanodiamond and multi-walled carbon nanotubes dual-reinforced aluminum matrix composite materials. *Materials Science and Engineering: A* **2015**, *632*, 72. **DOI:** 10.1016/j.msea.2015.02.057
13. Choi, H. J.; Min, B. H.; Shin, J. H.; Bae, D. H. Strengthening in nanostructured 2024 aluminum alloy and its composites containing carbon nanotubes. *Composites Part A: Applied Science and Manufacturing* **2011**, *42*, 1438. **DOI:** 10.1016/j.compositesa.2011.06.008
14. Deng, C.; Zhang, X.; Wang, D.; Lin, Q.; Li, A. Preparation and characterization of carbon nanotubes/aluminum matrix composites. *Materials Letters* **2007**, *61*, 1725. **DOI:** 10.1016/j.matlet.2006.07.119
15. Subramaniam, C.; Yamada, T.; Kobashi, K.; Sekiguchi, A.; Futaba, D. N.; Yumura, M.; Hata, K. One hundred fold increase in current carrying capacity in a carbon nanotube–copper composite. *Nature Communications* **2013**, *4*, 2202. **DOI:** 10.1038/ncomms3202
16. Kim, Y.; Lee, J.; Yeom, M. S.; Shin, J. W.; Kim, H.; Cui, Y.; Kysar, J. W.; Hone, J.; Jung, Y.; Jeon, S.; Han, S. M. Strengthening effect of single-atomic-layer graphene in metal–graphene nanolayered composites. *Nature Communications* **2013**, *4*, 2114. **DOI:** 10.1038/ncomms3114
17. Wu, Z.-S.; Zhou, G.; Yin, L.-C.; Ren, W.; Li, F.; Cheng, H.-M. Graphene/metal oxide composite electrode materials for energy storage. *Nano Energy* **2012**, *1*, 107. **DOI:** 10.1016/j.nanoen.2011.11.001
18. Brown, L.; Joyce, P.; Forrest, D.; Wolk, J. Physical and mechanical characterization of a nano carbon infused aluminum-matrix composite. *Proceedings of the SAMPE Fall Technical Conference* **2011**.
19. Nilufar, S.; Siddiqi, S.; Jasiuk, I. Multi-scale characterization of novel aluminum-carbon nanocomposites. *Materials Science & Technology Conference and Exhibition* **2012**
20. Jasiuk, I.; Nilufar, S.; Salamanca-Riba, L.; Isaacs, R.; Siddiqi, S. Novel aluminum-carbon materials. *Technical Proceedings of the 2013 NSTI Nanotechnology Conference and Expo* **2013**.
21. Salamanca-Riba, L.; Isaacs, R.; Mansour, A. N.; Hall, A.; Forrest, D. R.; LeMieux, M. C.; Shugart, J. V. A new type of carbon nanostructure formed within a metal-matrix. *Proceedings of Nanotech Conference and Expo* **2012**.
22. Forrest, D. R.; Jasiuk, I.; Brown, L.; Joyce, P.; Mansour, A.; Salamanca-Riba, L. *Novel metal-matrix composites with integrally-bound nanoscale carbon* **2012**.
23. Brown, L.; Joyce, P.; Forrest, D.; Salamanca-Riba, L. Physical and mechanical characterization of a nanocarbon infused aluminum-matrix composite. *ASTM Materials Performance Characterization* **2014**, 3(1), 65-80. **DOI:** 10.1520/MPC20130023
24. Knych, T.; Kwaśniewski, P.; Kiesiewicz, G.; Mamala, A.; Kawecki, A.; Smyrak, B. Characterization of nanocarbon copper composites manufactured in metallurgical synthesis process. *Metallurgical and Materials Transactions B* **2014**, *45*, 1196-1203. **DOI:** 10.1007/s11663-014-0046-7
25. Knych, T.; Kiesiewicz, G.; Kwasniewski, P.; Mamala, A.; Smyrak, B.; Kawecki, A. Fabrication and cold drawing of copper covetic nanostructured carbon composites/Otrzymywanie oraz ciągnienia kompozytów miedzianych typu covetic o strukturze nanometrycznej. *Archives of Metallurgy and Materials* **2014**, *59*, 1283-1286. **DOI:** 10.2478/amm-2014-0219
26. Salamanca-Riba, L. G.; Isaacs, R. A.; LeMieux, M. C.; Wan, J.; Gaskell, K.; Jiang, Y.; Wuttig, M.; Mansour, A. N.; Rashkeev, S. N.; Kuklja, M. M.; Zavalij, P. Y.; Santiago, J. R.; Hu, L. Synthetic crystals of silver with carbon: 3D epitaxy of carbon nanostructures in the silver lattice. *Advanced Functional Materials* **2015**, *25*, 4768-4777. **DOI:** 10.1002/adfm.201501156
27. Isaacs, R. A.; Zhu, H.; Preston, C.; Mansour, A.; LeMieux, M.; Zavalij, P. Y.; Jaim, H. M. I.; Rabin, O.; Hu, L.; Salamanca-Riba, L. G. Nanocarbon-copper thin film as transparent electrode. *Applied Physics Letters* **2015**, *106*, 193108. **DOI:** 10.1063/1.4921263
28. Ma, B.; Winarski, R.; Wen, J.; Miller, D.; Segre, C.; Balachandran, U.; Forrest, D. Investigation of carbon nanostructure in copper covetics by x-ray nanotomography. *Proceedings of the 2nd International Conference on Tomography of Materials and Structures* **2015**.
29. Jaim, H. M. I.; Isaacs, R. A.; Rashkeev, S. N.; Kuklja, M.; Cole, D. P.; LeMieux, M. C.; Jasiuk, I.; Nilufar, S.; Salamanca-Riba, L. G. Sp2 carbon embedded in Al-6061 and Al-7075 alloys in the form of crystalline graphene nanoribbons. *Carbon* **2016**, *107*, 56-66. **DOI:** 10.1016/j.carbon.2016.05.053
30. Balachandran, U.; Ma, B.; Dorris, S. E.; Koritala, R. E.; Forrest, D. R. Nanocarbon-infused metals: a new class of covetic materials for energy applications. *Materials Science & Technology Conference and Exhibition* **2016**.
31. Jaim, H. M. I.; Cole, D. P.; Salamanca-Riba, L. G. Characterization of carbon nanostructures in Al and Ag covetic alloys. *Carbon* **2017**, *111*, 309-321. **DOI:** 10.1016/j.carbon.2016.10.007